Binder and monomer valencies determine the extent of collapse and reswelling of chromatin

Sougata Guha[1,2]
[1]*Department of Physics, Indian Institute of Technology Bombay, Mumbai 400076, India*
[2]*INFN Napoli, Complesso Universitario di Monte S. Angelo, Napoli 80126, Italy*
Email : guha@na.infn.it

Multivalent binding protein mediated collapse of chromatin polymer has long been established as one of the driving factors in chromatin organisation inside cells. These multivalent proteins can bind to distant binding sites along the chromatin backbone and bring them together in spatial proximity, leading to collapsed conformations. Recently, it has been suggested that these proteins not only drive collapse of the chromatin polymer, but also reswelling at higher concentrations. In this study, we investigate the physical mechanisms underlying this unexpected reswelling behaviour. We use Langevin dynamics simulation of a coarse-grained homopolymer to investigate the effects of the valencies of both the binders and the monomers on the polymer conformations. We found that while the extent of collapse of the polymer is strongly dependent on the binder valency, the extent of reswell is largely determined by the monomer valency. Furthermore, we also discover two different physical mechanisms that drive reswelling of the polymer - *excluded volume effects* and *loss of long-range loops*. Finally, we obtain a phase diagram to determine the regimes where either of these mechanisms are the dominant factor leading to polymer reswelling.

I. INTRODUCTION

Understanding the physical principles behind the spatial and temporal organisation of chromatin inside the nucleus remains a central challenge. Dynamic chromatin organisation is critical for ensuring proper gene regulation and perturbations in this assembly can lead to various diseases [1–6]. Recent developments in experimental techniques, known as 3C, 4C, 5C, Hi-C and micro-C have provided deep insights on the importance of chromosome contacts in chromatin organisation [7–14]. These experiments have revealed the hierarchical organisation of chromatin at multiple scales, through the formation of Topologically Associated Domains (TADs) and A/B compartments [15]. At larger scales, each chromosome occupies a specific region, known as chromosome territory, within the nucleus and is confined due to the surrounding chromosomes [15].

Formation of chromatin loops is one of the ubiquitous structural motifs across cell types and these loops are formed by different chromatin-binding proteins [16–18]. These proteins bind to different segments of chromatin which are separated by a long distance along the chromatin chain and bring them spatially close to each other [19–24]. Long loops, driven by the Structural Maintenance of Chromatin (SMC) proteins such as cohesin and condensin, localise to TAD boundaries, and ensure insulation among neighbouring TADs. Chromatin organisation driven by loops are known to be spatially and temporally dynamic [25–27] and vary depending on several factors, such as chromatin epigenetic states [28, 29], and cell cycle states [30, 31]. Chromatin loops are also crucial in regulating various biological processes. Specific loops like TAD boundaries have been implicated to facilitate enhancer-promoter interactions [32–34] which is necessary for gene activation and DNA replication [20, 35].

A critical factor underlying the formation of these loops is the interaction of the chromatin with various DNA-binding proteins. These proteins are often multivalent i.e. they can bind to different number of chromatin segments simultaneously. For example cohesin and condensin crosslink chromatin segments and bring them spatially close to each other [7, 32, 36–38]. HP1 proteins are known to interact with methylated histone H3 [39, 40] and are also reported to vary its valency through self oligomerisation [41, 42]. Also, polycomb proteins (PRC1) are known to bring multiple DNA segments containing PRC1-binding domains together [43]. Patchy particles with limited valency have also been studied in both simulations [44, 45] and experiments [46, 47], as well as in the context of chromatin organisation [48]. Additionally, chromatin can also exhibit multivalency to many proteins. For example, PRC complexes bind to H2A or H3 histone proteins [49]. As each nucleosome consists of a pair of these histone proteins, nucleosomes itself is bivalent to polycomb protein complexes. Also, in zebrafish sperms, developmental genes are packed in large blocks of chromatin which contains multiple binding sites of post-translational modification complexes [50]. Moreover, in a coarse-grained polymer picture of chromatin, each monomer consists of a chromatin segment which varies from nucleosome level ($\sim 200bp$) [51, 52] to 100 kbp [53]. These segments usually contain multiple binding domains for different proteins and the number of such domains (i.e chromatin valency) depends on the specific chromatin segment and the scale of coarse-graining. Therefore, understanding the impact of varying protein and chromatin valencies is critical in comprehending the processes of chromatin compaction and reswelling.

Polymer based models of chromatin have yielded numerous insights into this process of protein-chromatin interactions and their role in regulating chromosome organisation [53–71]. A foundational model is the 'Strings and Binders Switch' (SBS) model [72, 73]. In this model, chromatin is assumed as a self-avoiding polymer which consists binding sites for diffusible binding proteins. Diffusible binding proteins dynamically attach to distant segments of the chromatin polymer and hence form loops. Due to this long-range bridging of chromatin segments, chromatin polymer collapses and undergoes a coil-globule transition [56]. The transition point is known to be a function of binder concentration and chromatin-binder affinity [53]. The contact probability exponent and the polymer size exponents obtained in this model match very well with the experimentally observed exponents [74]. Subsequently, several variants of this model have been implemented in the context of chromatin organisation inside cell nucleus. For example, incorporating the active and inactive epigenetic states of chromatin along with the chromatin semi-flexibility leads to different collapsed structure of the chromatin clusters [57–59]. Presence of specific binding domains for different binders has been used to reproduce TADs and sub-TADs

observed experimentally [67, 75]. Many studies have also used binder-mediated bridging implicitly by considering intra-polymer crosslinking and explained various features of chromatin organisation [61, 62, 76–81].

In a previous study [82], we investigated role of diffusible multivalent binders on chromatin organisation in confined systems. We reported that chromatin-protein interactions can not only drive polymer compaction, but can also reswell the polymer at higher concentrations. Additionally, the amount of reswell, the required binder concentration for reswelling and the timescales are found to depend on the scale of confinement. This counterintuitive reswelling of the polymer has also been reported in other polymer models [83, 84]. A critical factor in understanding this collapse, and subsequent reswelling, is the interplay of binder and monomer valencies. These determine the underlying looping kinetics, and hence, determine the structural properties of the chromatin polymer. In this work, we systematically study the effect of both the valency of the binding protein and the monomer itself on the polymer conformations and spatial organisation.

II. MODEL

To understand how this choice of the valencies of both monomers and binders affect the collapse and reswell of the chromatin polymer we study a polymer-binder system under confinement. We choose a polymer of length 512 spherical monomers with diameter σ. The polymer chain connectivity is maintained by introducing FENE potential [85] between consecutive monomers and is given by

$$U_{FENE}(r_{i+1,i}) = -\frac{k_{FENE}}{2} R^2_{FENE} \ \ln[1-(r_{i+1,i}/R_{FENE})^2] \tag{1}$$

where $k_{FENE} = 30k_BT$ [85] is the spring constant, $R = 1.6\sigma$ [85] is the maximum allowed bond length and $r_{i,j} = |r_i - r_j|$ is the euclidean distance between the ith and j^{th} monomers. All non-bonded monomers interact via volume exclusion modelled as purely repulsive WCA potential [86],

$$U_{WCA} = \begin{cases} 4\epsilon[(\sigma/r_{i,j})^{12} - (\sigma/r_{i,j})^6] + \epsilon & \text{for} \ \ r_{i,j} < 2^{1/6}\sigma \\ 0 & \text{otherwise} \end{cases} \tag{2}$$

The interaction strength ϵ is chosen to be equal to k_BT.

The individual binders are modelled as spherical beads of diameter σ. While the binders mutually interacts via exluded volume interaction, the polymer-binder interaction is modelled as 'Truncated and Shifted Lennard-Jones' (TSLJ) potential,

$$U_{TSLJ}(r) = \begin{cases} U_{LJ}(r) - U_{LJ}(r_c) & \text{for} \ \ r < r_c \\ 0 & \text{otherwise} \end{cases} \tag{3}$$

where $U_{LJ}(r) = 4\epsilon_m[(\sigma/r)^{12} - (\sigma/r)^6]$ with $\epsilon_m = 3.5\epsilon$ [82] and $r_c = 1.5\sigma$ [82]. This interaction is permitted as long as both monomer and the binder have not saturated its valency i.e., monomer is bound to a number of binder and binder is bound to a number of monomer less than their own valencies. If either of the monomer and the binder has already saturated its valency then they interact via volume exclusion. To ensure monomer-binder bonding follow valency restriction we make a 'probable list' of monomers around binders and the binders bind with randomly chosen monomers from that list in accordance with its valency restriction (see Ref. [82] for more details). In this case, we only include those monomers that have not already utilized all their valencies into the 'probable list'.

We implement the confinement as a spherical wall of radius R which interacts with all particles via WCA potential. In this paper, we keep the chromatin volume density or confinement radius fixed and choose a confinement radius which corresponds to a chromatin volume density, $\phi \sim 0.044$ which is consistent with experimentally observed chromatin density inside the nucleus that varies in the range $\phi = 0.01 - 0.25$[87]. We also keep the binder number density (c) within biologically relevant regime [82, 88]. Here, we investigate the chromatin polymer conformations at different binder and monomer valencies. We discard the mono-valency of binders as in such case formation of loops would not be possible which would lead to no compaction of the polymer.

III. RESULTS

Firstly, we characterise how binder and monomer valencies impact the extent of compaction and reswelling of the chromatin polymer. As the amount of compaction and reswelling differ for different BV and MV values, we introduce a compaction parameter Ω to denote the extent of compaction/reswelling. The compaction parameter represents fractional extent of compaction/reswelling compared to the maximum compaction observed for a given values of BV and MV and can be expressed as

$$\Omega = \frac{\langle R_g \rangle - \langle R_g^c \rangle}{\langle R_g^0 \rangle - \langle R_g^c \rangle}$$

where $\langle R_g^0 \rangle$ is the average radius of gyration in absence of any binders and $\langle R_g^c \rangle$ is the lowest average R_g value (maximum compaction) for a given BV and MV values.

Fig. 1 shows the variation of R_g and Ω with binder number N_b and binder concentration (c), respectively, for different binder valencies (BV) at fixed monomer valencies (MV). Note that for any monomer valency, the polymer size (R_g) decreases with increasing binder valency for all binder numbers, as shown in Fig. 1a-c. Increasing BV leads to an effective monomer cloud around binders where each binder binds to multiple monomers which surround the binder itself. This monomer cloud drives the polymer to higher compaction. For low binder valency (BV=2), there is no significant compaction of the polymer irrespective of monomer valency. This is due to the fact that when binders bind to one monomer, it is highly likely for the binder to exhaust its valency by binding to another monomer that is sequentially close along the polymer backbone to the already bound monomer. Hence most of the loops are short-ranged and lack of long-ranged loops lead to no compaction of the polymer. Although the reswelled R_g of the polymer varies for different values of BV and MV (Fig. 1a-c), interestingly, the fractional reswelling of the polymer (denoted by compaction parameter Ω) for BV≥ 4 has similar values for a given value of MV as shown in Fig. 1d-f. Therefore, irrespective of the monomer valency, the polymer compaction (and not the reswelling) predominantly depends on the binder valency and the extent of compaction increases with increasing the binder valency.

To understand the impact of monomer valency on polymer conformation, we now study the variation of R_g and Ω as a function of N_b and c, respectively, for different MV values for a fixed BV (Fig. 2). As mentioned earlier, for BV=2, there is a minor compaction of the polymer (Fig.

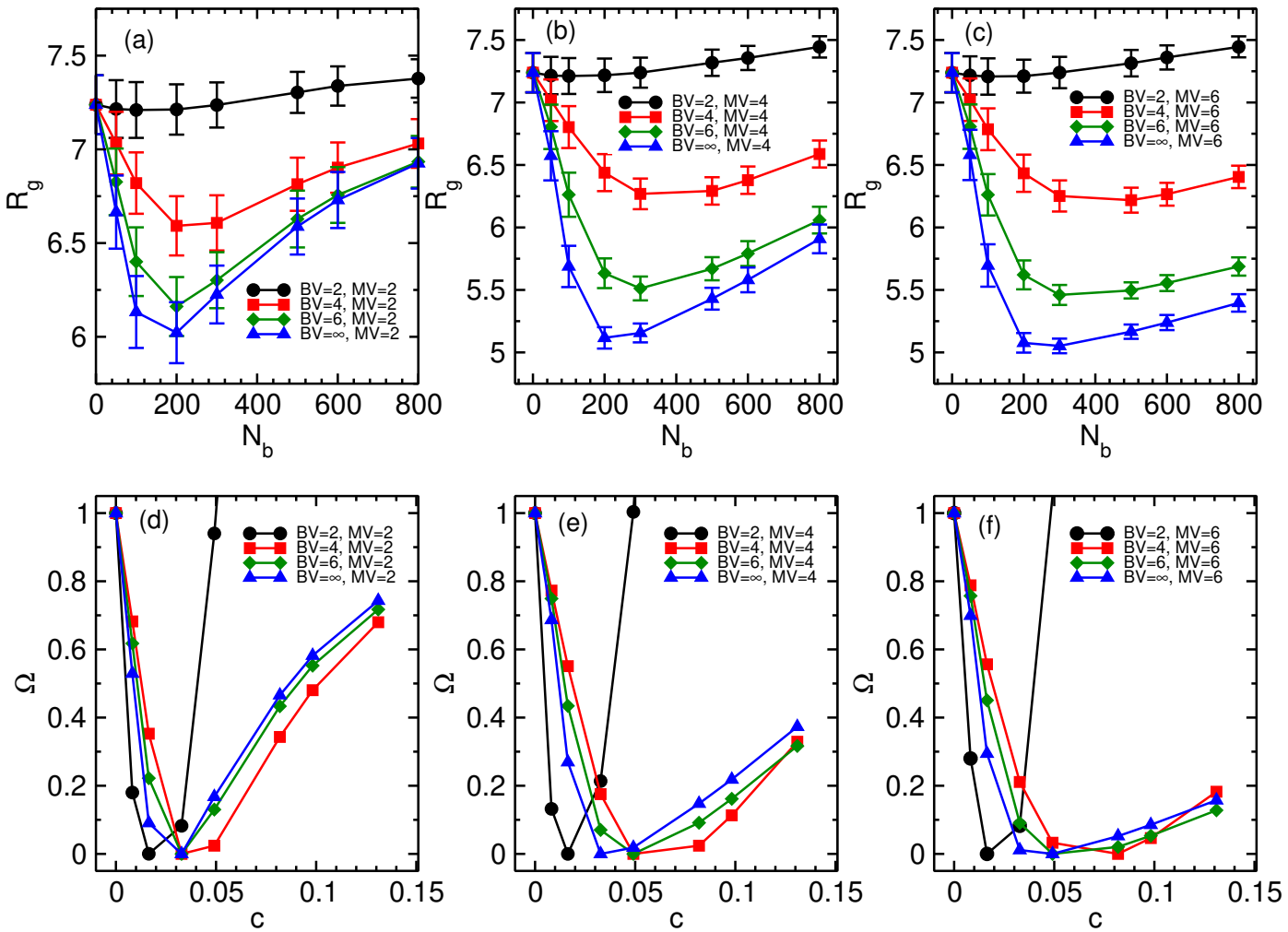

FIG. 1: Comparison of variation in R_g as a function of N_b for different binder valencies at fixed monomer valency. Top panels (a-c) shows the variation of R_g as a function of N_b for three different monomer valencies. Each panel compares the the R_g variation for different binder valencies at a fixed monomer valency. The bottom panels (d-f) depict the variation of the compaction parameter (Ω) with binder number density (c) corresponding to the same binder and monomer valencies as in the top panels.

2a). Surprisingly, the polymer R_g, for BV=2, varies identically for MV$\geq$ 4. For higher binder valencies (BV$\geq$ 4), the extent of polymer compaction increases as monomer valency is increased, but the reswelling considerably decreases with increasing monomer valencies, as shown in Fig. 2b and 2c. This is also reflected in the corresponding Ω vs c plots shown in Fig. 2d-f. Note that the high value of Ω in BV=2 case (Fig. 2d) is an artifact due to the minimal compaction of the polymer. Converse to the compaction, the extent of reswelling of the polymer predominantly depends on monomer valency as is evident from Fig. 2. Interestingly, the monomer valency has opposite effects on reswelling depending on the value of binder valency. For high binder valency (BV$\geq$ 4), the value of polymer R_g is lower for higher monomer valencies (Fig. 2b-c). However, for binder valency (BV=2), the R_g of the reswollen polymer is higher for higher monomer valencies (MV$\geq$ 4) than the reswollen polymer R_g in case of MV=2 (Fig. 2a).

To understand these opposite effects of monomer valency on polymer reswelling, we now look into the loop size distribution of the system. Specifically, we compare the loop size distributions for the highest number of binders used in our study (N_b = 800) across different binder valency (BV) and monomer valency (MV). We found that for a given monomer valency, increasing binder valency leads to an increase in the number of loops (Fig. 3a-c) and hence the R_g is lower for higher binder valency. A similar increase in loop number is observed with increasing MV values for BV$\geq$ 4 (Fig. 3e-f). However, when binder valency is low (BV=2), the loop distribution remains relatively unchanged across different monomer valencies (Fig. 3d). The very low number of long-ranged loops in this case indicates that the reswelling is due to the excluded volume of binders which induces an effective repulsive force between the binders that are bound to the polymer. This can be visualised as an effective binder cloud formed around the monomers due to multiple binders binding to same monomer. Interestingly, while the R_g remains almost identical for higher monomer valencies (MV$\geq$ 4), the amount of reswelling in case of MV=2 is lower than the reswelling observed in cases of MV$\geq$ 4 (Fig. 2a). This can be thought of as follows: in case of MV=2, the binder cloud formed by only two binders can not efficiently exclude the volume, and the volume excluded by two binder clouds can overlap as schematically shown in Fig. 3g. With higher monomer valency, the binder cloud formed by binders around monomers efficiently excludes volumes larger than the individual monomer volume and volumes occupied by the binder clouds can not overlap (Fig. 3h). This efficient volume exclusion by binder clouds in case of higher monomer valencies increases the effective volume occupied by each monomer and hence reswells the polymer.

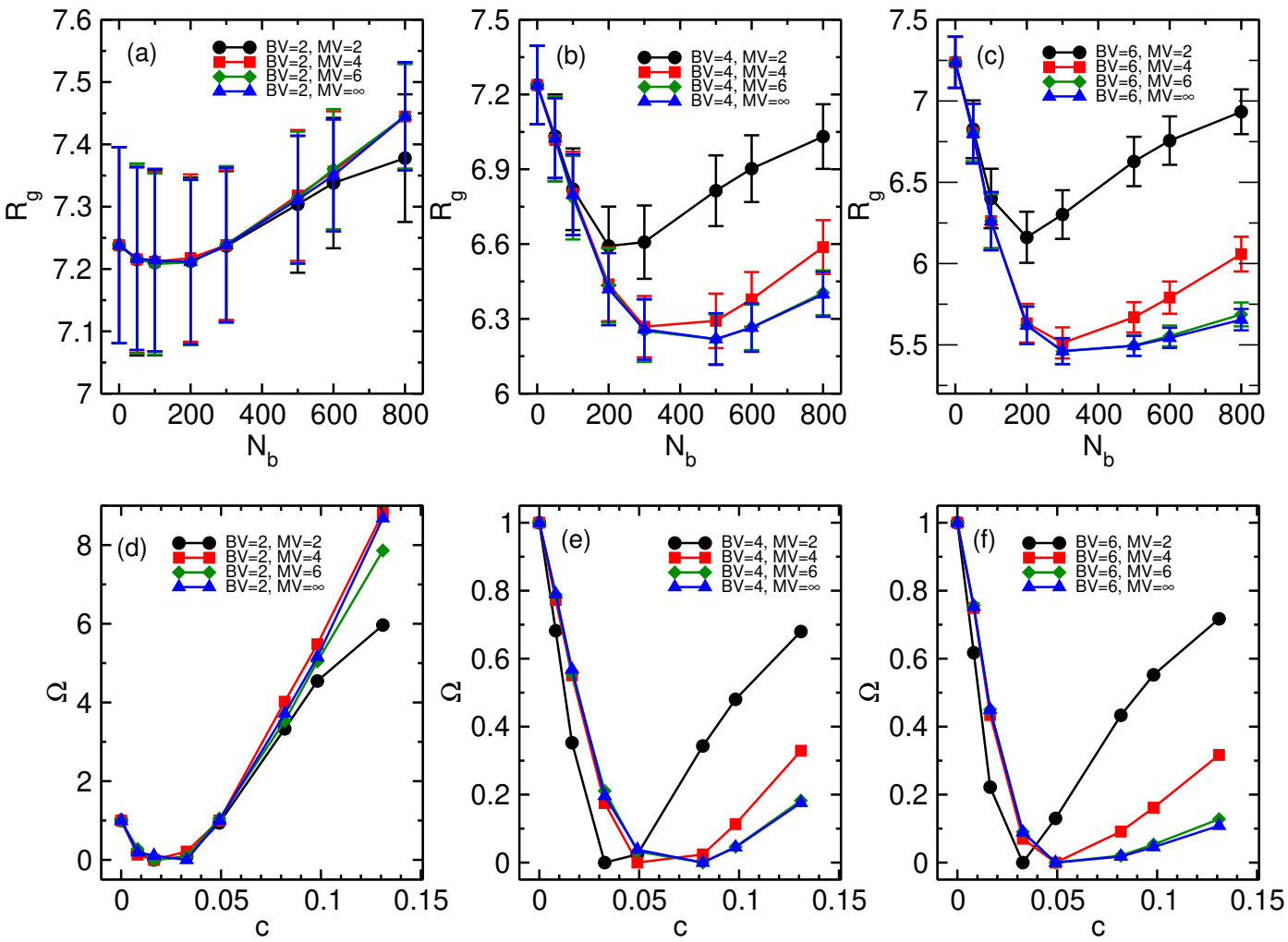

FIG. 2: Comparison of variation in R_g as a function of N_b for different monomer valencies at fixed binder valency. Top panels (a-c) shows the variation of R_g as a function of N_b for three different binder valencies. Each panel compares the the R_g variation for different monomer valencies at a fixed binder valency. The bottom panels (e-f) depict the variation of the compaction parameter (Ω) with binder number density (c) corresponding to the same binder and monomer valencies as in the top panels.

The more efficient volume exclusion by binder clouds for MV$\geq$ 4 leads to higher R_g than in the case of MV=2. But with higher binder valency (BV$\geq$ 4), the number of long loops increases with increasing monomer valency (Fig. 3e-f) and hence the extent of polymer compaction is more for higher monomer valencies (Fig. 2b-c). Due to the increase in the number of long loops with increasing monomer valencies, the extent of reswelling in this case also diminishes.

Next we plot the loop size distribution for three different binder numbers each corresponding to a different chromatin conformations - semi-open, fully collapsed and reswelled (Fig. 4a and 4b). As the amount of reswell is different for different valencies, we compare the reswelled polymer configuration at same binder number ($N_b = 800$). Interestingly, for a given binder and monomer valency, two distinct causes of reswelling emerge. One is that reswelling is driven by the loss of long loops at higher N_b, while the other is predominantly due to the excluded volume of the binder cloud around each monomer. In the first scenario, when the binder number is low (semi-open polymer configurations), there are fewer long loops. However, as the binder number increases, leading to a fully collapsed polymer conformation, the number of loops, both long-ranged and short-ranged, increases significantly(Fig. 4a). Due to this increase in long-ranged loops the polymer collapses and reaches minimum R_g. As the binder number is increased further, the number of long-ranged loops diminishes. This can be understood as follows: binder association with the polymer occurs on two distinct timescales. Initially, at very short times, binders rapidly form short-ranged loops by binding with monomers that are sequentially close. These short-ranged loops form almost immediately when a binder comes into proximity with a monomer. At longer timescales, the binders that are already bound to a monomer may crosslink with another monomer from a distant segment of the polymer, leading to the formation of long-ranged loops. When the number of binders is high, there are enough binders available to satisfy the valencies of all monomers at short timescales by forming short-ranged loops. Because the valencies of nearly all monomers are saturated at these short timescales, the likelihood of forming long-ranged loops, which typically occur at longer timescales, is greatly reduced. This is evident in the significant decrease in long-ranged loops observed when the binder number is increased from $N_b = 200$ to $N_b = 800$, while the number of short-ranged loops remains nearly unchanged (Fig. 4a). Hence, this reduction of long-ranged loops at high binder numbers leads to a semi-open state of the polymer which corresponds to higher R_g, i.e, the polymer reswells. In contrast, when reswelling of the

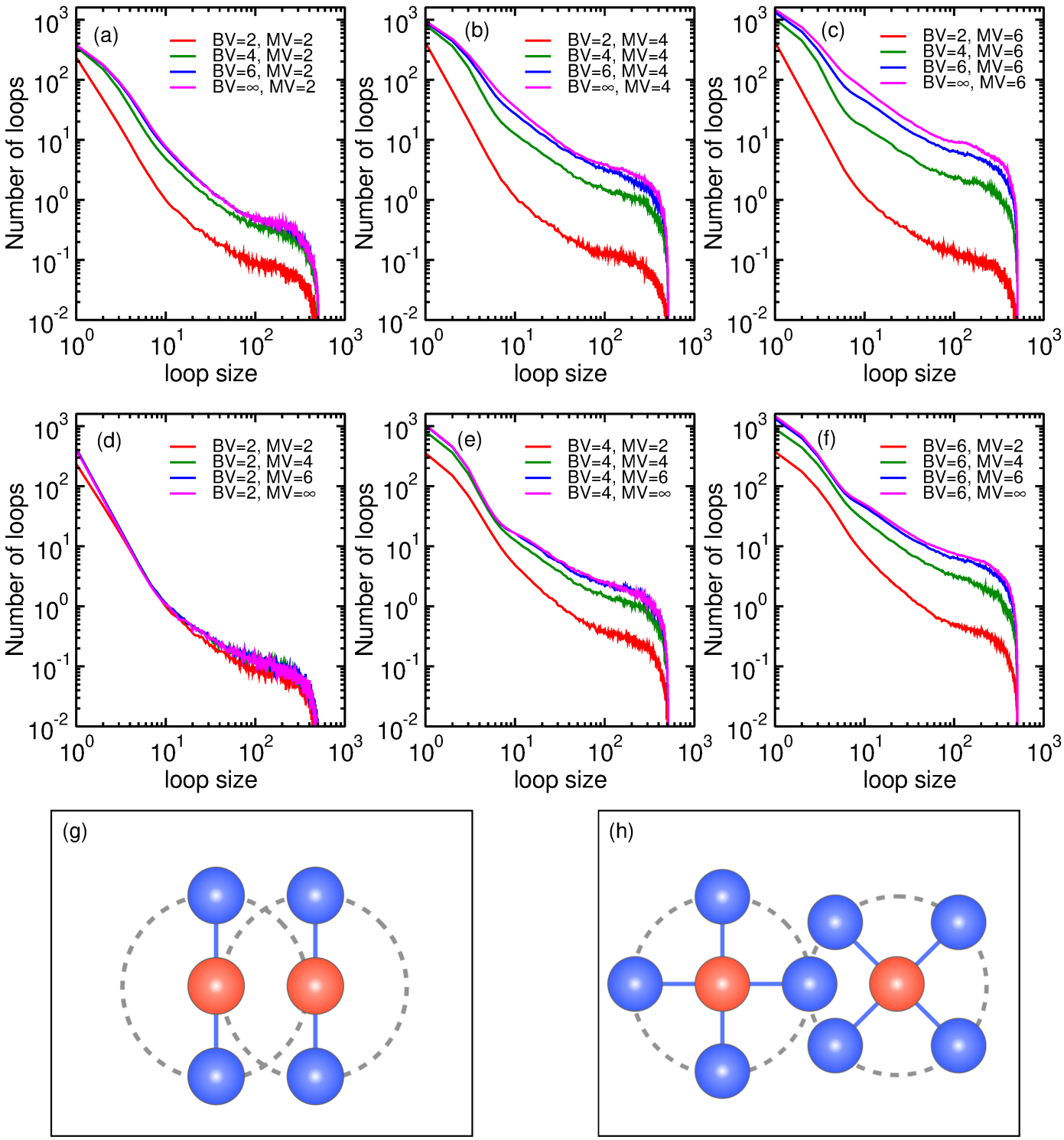

FIG. 3: Loop distribution for different binder and monomer valencies for $N_b = 800$. Panels (a-c) compare the loop size distribution for different binder valencies for 3 fixed monomer valencies, whereas panels (d-f) compare the same for different monomer valencies for 3 fixed binder valencies. Panels (g) and (h) show the excluded volume effects by 2 binders (denoted by blue beads) bound to each monomers and 4 binders bound to each monomers (denoted by red beads), respectively.

polymer is dominated by excluded volume effects, the number of long-ranged as well as short-ranged loops monotonically increase with increasing binder number (Fig. 4b). This increase in loop number across all loop sizes indicates an increase in the total number of binders within the volume occupied by the polymer. As a result of the mutual repulsion between binders within the polymer's occupied volume, the polymer undergoes reswelling. Interestingly, at even higher binder numbers, this reswelling caused by excluded volume effects reaches a saturation point, after which further polymer reswelling is once again dominated by the loss of loops. As illustrated in Fig. 4c, when the binder number is increased from $N_b = 300$ (corresponding to the fully compacted conformation) to $N_b = 500$, the number of loops increases, suggesting that reswelling in this case is primarily driven by excluded volume effects. However, as the binder number increases further to $N_b = 800$, the number of long-ranged loops decreases, as shown in the inset of Fig. 4c. Consequently, the additional reswelling of the polymer from $N_b = 500$ to $N_b = 800$ is clearly domi-

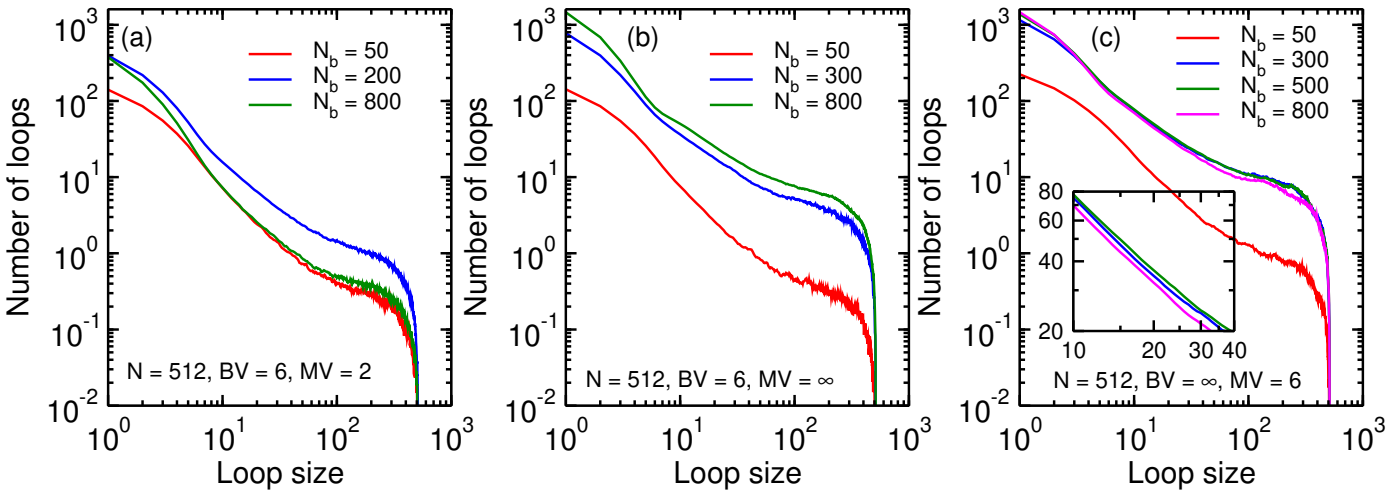

FIG. 4: Loop size distribution for different binder and monomer valencies. Panel (a) shows a re-entrant like behaviour in loop size distribution with increasing binder number while panel (b) shows a monotonic increase in number of loops with increasing binder numbers. Panel (c) depicts the transition of excluded volume-driven reswelling into reswelling driven by loss of loops. The inset in panel (c) shows a zoomed-in picture of the loop distribution and clearly show the loss of loops.

nated by the loss of loops.

Now that we've identified two distinct physical mechanisms responsible for polymer reswelling, we plot a phase diagram to distinguish the dominant mechanism of reswelling for different combinations of binder and monomer valencies (Fig. 5). It is to be noted that the two mechanisms are not mutually exclusive and both contribute simultaneously in the polymer reswelling as previously described in Fig. 4c. We thus define a numerical threshold to distinguish the phases depending on the dominant cause of the reswelling for a given set of binder and monomer valencies. As at very high binder numbers all reswelling are expected to be dominated by loss of loops, we restrict our phase diagram to the binder number $N_b = 800$ (equivalent to binder volume density $\phi_b \sim 0.7$ and binder number density $c \sim 0.13$). Therefore in the presence of 800 binders, if the number of loops is lower than the number of loops at lower binder numbers, $N_b = 600$ ($\phi_b \sim 0.5$ and $c \sim 0.13$), then we call it a loop loss phase, and if the number of loops monotonically increases till $N_b = 800$ then we call it excluded volume phase. As discussed earlier, for BV=2, the number of long loops are low and hence, as expected, we found that the reswelling in this case is dominated by excluded volume effects. We also found that reswelling dominated by the loss of loops is prevalent in lower monomer valencies while at higher monomer valencies, reswelling is predominantly driven by excluded volume effects.

IV. DISCUSSION

Several polymer models have been studied in literature in the context of chromatin organisation. While chromatin compaction is well understood using polymer folding in presence of multivalent bridging molecules, very little is known regarding the role of these bridging proteins in reswelling the chromatin. In our previous work [82], we have shown that these multivalent binders can both compact and reswell the chromatin polymer under confinement. Also, a chromatin monomer can have multiple binding sites for these proteins, making the polymer multivalent. Therefore, it is important to understand how the valencies of binders and monomers affect the compaction and reswelling of the chromatin under confinement.

In this work, we have shown that the binder and monomer valencies can play a crucial role in chromatin organisation inside cell nucleus. We have found that the extent of chromatin compaction increases with increasing binder valency. Additionally, we do not observe any significant compaction of the polymer in the case of binder valency 2 as in this case most loops are short-ranged and lack of long-ranged loops results in no compaction. The polymer still shows a reswelling at higher binder numbers for binder valency 2. This reswelling of polymer is found to be less for monomer valency 2, while for higher monomer valencies the reswelling is identical and higher than the reswelling for monomer valency 2. On the other hand, the extent of reswelling is found to diminish with the increasing monomer valency for higher binder valencies. We then further quantified the loop size distributions to understand this contrasting behaviour of polymer size for different monomer valencies. We show that in one case the number of long-ranged loops monotonically increase with incrasing binder number, while in other case the loop size distributions show a non-monotonic behaviour with increasing binder numbers. We conclude that the reswelling of the polymer is driven by two factors - excluded volume effects of the binders and lack of long-ranged loops at higher binder numbers. While the monotonic increase in number of loops contribute to the increasing excluded volume effects and the non-monotonic variation of loop distribution indicates a loss of loops at higher binder numbers. Based on these features we obtain a phase diagram separating two causes of reswelling as a function of monomer and binder valencies. We have found that at higher binder valency and lower monomer valency regime the reswelling is predominantly driven by loss of long-ranged loops, while in the other regimes reswelling is driven by excluded volume effects. Finally, we also have shown that at even higher binder numbers, excluded volume driven reswelling saturates and further reswelling with increasing binder number is dominated by loss of long-ranged loops.

This differential causes of reswelling for different binder and monomer valencies can have important biological implications. Different experimental studies have reported

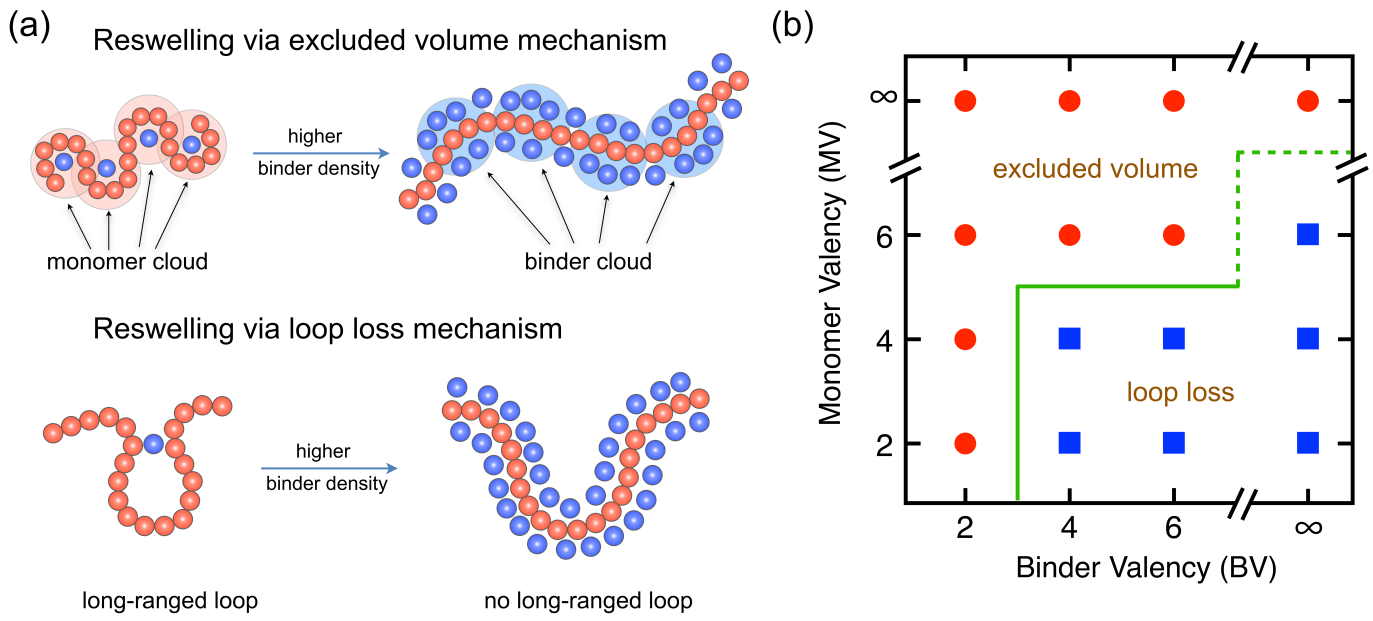

FIG. 5: Distinct mechanisms of polymer reswelling. Panel (a) shows schematic representation of two mechanisms of polymer reswelling. Red chain denotes the polymer and the blue beads depict the binders. Panel (b) shows a phase diagram distinguishing the two regimes of reswelling mechanism on binder valency-monomer valency plane. Circles (red) denote reswelling due to excluded volume while squares (blue) denote reswelling due to loss of long-ranged loops. The dashed (green) line denotes the phase boundary between the two phases.

that various DNA-associated proteins have different sizes ranging from $10nm$ to a few hundred nm [49, 89]. Furthermore, transcription factors are known to aggregate near its binding sites and form large transcriptional condensates [90–92]. In case of excluded volume-dominated reswelling, the size of the binder proteins or transcriptional condensates would play a crucial role. Larger proteins or condensates exclude larger volume and thus the polymer reswelling would be larger, while a smaller protein or condensate would exclude less volume and the reswelling would not be as significant as in case of bigger proteins. On the other hand, when reswelling is dominated by loss of loops, the extent of reswelling is independent of protein size. Certainly, future experiments that specifically focus on the number of loops can provide valuable insights into the underlying physical mechanisms responsible for chromatin reswelling in the presence of particular DNA-associated proteins. By systematically varying the binder and monomer valencies and observing the resulting changes in chromatin compaction and reswelling, researchers can gain a deeper understanding of the specific factors driving these processes. This knowledge can help elucidate the roles of different DNA-associated proteins and their interactions with chromatin in the stability and dynamics of chromatin organisation.

CONFLICTS OF INTEREST

There are no conflicts to declare.

ACKNOWLEDGEMENTS

I would like to thank Dr. Mithun K. Mitra and Shuvadip Dutta for their valuable discussions and detailed feedback on the manuscript. I also acknowledge the computing facilities and partial financial support provided by IIT Bombay. Additionally, I would like to express my gratitude to INFN Napoli for their financial support through the "Post-doctoral Senior Level 3 Research Grant in Theoretical Physics (2022)".

DATA AVAILABILITY STATEMENT

The data that support the findings of this study are available from the corresponding author upon reasonable request.

[1] Darío G Lupiáñez, Katerina Kraft, Verena Heinrich, Peter Krawitz, Francesco Brancati, Eva Klopocki, Denise Horn, Hülya Kayserili, John M Opitz, Renata Laxova, et al. Disruptions of topological chromatin domains cause pathogenic rewiring of gene-enhancer interactions. *Cell*, 161(5):1012–1025, 2015.

[2] Shipra Bhatia, Hemant Bengani, Margaret Fish, Alison Brown, Maria Teresa Divizia, Riccardo De Marco, Guiseppe Damante, Robert Grainger, Veronica Van Heyningen, and Dirk A Kleinjan. Disruption of autoregulatory feedback by a mutation in a remote, ultra-conserved pax6 enhancer causes aniridia. *The American Journal of Human Genetics*, 93(6):1126–1134, 2013.

[3] Laura A Lettice, Simon JH Heaney, Lorna A Purdie, Li Li, Philippe De Beer, Ben A Oostra, Debbie Goode, Greg Elgar, Robert E Hill, and Esther de Graaff. A long-range shh enhancer regulates expression in the developing limb and fin and is associated with preaxial polydactyly. *Human*

molecular genetics, 12(14):1725–1735, 2003.

[4] Bryan M Turner. Epigenetic responses to environmental change and their evolutionary implications. *Philosophical Transactions of the Royal Society B: Biological Sciences*, 364(1534):3403–3418, 2009.

[5] Zheng Wang, Renzhi Cao, Kristen Taylor, Aaron Briley, Charles Caldwell, and Jianlin Cheng. The properties of genome conformation and spatial gene interaction and regulation networks of normal and malignant human cell types. *PloS one*, 8(3):e58793, 2013.

[6] Jeong Hyun Ahn, Eric S Davis, Timothy A Daugird, Shuai Zhao, Ivana Yoseli Quiroga, Hidetaka Uryu, Jie Li, Aaron J Storey, Yi-Hsuan Tsai, Daniel P Keeley, et al. Phase separation drives aberrant chromatin looping and cancer development. *Nature*, 595(7868):591–595, 2021.

[7] Erez Lieberman-Aiden, Nynke L Van Berkum, Louise Williams, Maxim Imakaev, Tobias Ragoczy, Agnes Telling, Ido Amit, Bryan R Lajoie, Peter J Sabo, Michael O Dorschner, et al. Comprehensive mapping of long-range interactions reveals folding principles of the human genome. *science*, 326(5950):289–293, 2009.

[8] Job Dekker, Karsten Rippe, Martijn Dekker, and Nancy Kleckner. Capturing chromosome conformation. *science*, 295(5558):1306–1311, 2002.

[9] Job Dekker. The three'c's of chromosome conformation capture: controls, controls, controls. *Nature methods*, 3(1):17–21, 2006.

[10] Luca Giorgetti and Edith Heard. Closing the loop: 3c versus dna fish. *Genome biology*, 17(1):1–9, 2016.

[11] Marieke Simonis, Petra Klous, Erik Splinter, Yuri Moshkin, Rob Willemsen, Elzo De Wit, Bas Van Steensel, and Wouter De Laat. Nuclear organization of active and inactive chromatin domains uncovered by chromosome conformation capture–on-chip (4c). *Nature genetics*, 38(11):1348–1354, 2006.

[12] Zhihu Zhao, Gholamreza Tavoosidana, Mikael Sjölinder, Anita Göndör, Piero Mariano, Sha Wang, Chandrasekhar Kanduri, Magda Lezcano, Kuljeet Singh Sandhu, Umashankar Singh, et al. Circular chromosome conformation capture (4c) uncovers extensive networks of epigenetically regulated intra-and interchromosomal interactions. *Nature genetics*, 38(11):1341–1347, 2006.

[13] Josée Dostie, Todd A Richmond, Ramy A Arnaout, Rebecca R Selzer, William L Lee, Tracey A Honan, Eric D Rubio, Anton Krumm, Justin Lamb, Chad Nusbaum, et al. Chromosome conformation capture carbon copy (5c): a massively parallel solution for mapping interactions between genomic elements. *Genome research*, 16(10):1299–1309, 2006.

[14] Tsung-Han S Hsieh, Assaf Weiner, Bryan Lajoie, Job Dekker, Nir Friedman, and Oliver J Rando. Mapping nucleosome resolution chromosome folding in yeast by micro-c. *Cell*, 162(1):108–119, 2015.

[15] Tom Misteli. The self-organizing genome: principles of genome architecture and function. *Cell*, 183(1):28–45, 2020.

[16] MPF Marsden and UK Laemmli. Metaphase chromosome structure: evidence for a radial loop model. *Cell*, 17(4):849–858, 1979.

[17] William C Earnshaw and Ulrich K Laemmli. Architecture of metaphase chromosomes and chromosome scaffolds. *The Journal of cell biology*, 96(1):84–93, 1983.

[18] James R Paulson and UK Laemmli. The structure of histone-depleted metaphase chromosomes. *Cell*, 12(3):817–828, 1977.

[19] Kyoichi Isono, Takaho A Endo, Manching Ku, Daisuke Yamada, Rie Suzuki, Jafar Sharif, Tomoyuki Ishikura, Tetsuro Toyoda, Bradley E Bernstein, and Haruhiko Koseki. Sam domain polymerization links subnuclear clustering of prc1 to gene silencing. *Developmental cell*, 26(6):565–577, 2013.

[20] Stefan Schoenfelder, Robert Sugar, Andrew Dimond, Biola-Maria Javierre, Harry Armstrong, Borbala Mifsud, Emilia Dimitrova, Louise Matheson, Filipe Tavares-Cadete, Mayra Furlan-Magaril, et al. Polycomb repressive complex prc1 spatially constrains the mouse embryonic stem cell genome. *Nature genetics*, 47(10):1179–1186, 2015.

[21] Sharmistha Kundu, Fei Ji, Hongjae Sunwoo, Gaurav Jain, Jeannie T Lee, Ruslan I Sadreyev, Job Dekker, and Robert E Kingston. Polycomb repressive complex 1 generates discrete compacted domains that change during differentiation. *Molecular cell*, 65(3):432–446, 2017.

[22] Jibak Lee. Roles of cohesin and condensin in chromosome dynamics during mammalian meiosis. *Journal of Reproduction and Development*, 59(5):431–436, 2013.

[23] Frank Uhlmann. Smc complexes: from dna to chromosomes. *Nature reviews Molecular cell biology*, 17(7):399–412, 2016.

[24] Kobe C Yuen and Jennifer L Gerton. Taking cohesin and condensin in context. *PLoS genetics*, 14(1):e1007118, 2018.

[25] Haitham A Shaban and Andrew Seeber. Monitoring the spatio-temporal organization and dynamics of the genome. *Nucleic acids research*, 48(7):3423–3434, 2020.

[26] Tadasu Nozaki, Ryosuke Imai, Mai Tanbo, Ryosuke Nagashima, Sachiko Tamura, Tomomi Tani, Yasumasa Joti, Masaru Tomita, Kayo Hibino, Masato T Kanemaki, et al. Dynamic organization of chromatin domains revealed by super-resolution live-cell imaging. *Molecular cell*, 67(2):282–293, 2017.

[27] Eloise I Prieto and Kazuhiro Maeshima. Dynamic chromatin organization in the cell. *Essays in biochemistry*, 63(1):133–145, 2019.

[28] Marit W Vermunt, Di Zhang, and Gerd A Blobel. The interdependence of gene-regulatory elements and the 3d genome. *Journal of Cell Biology*, 218(1):12–26, 2019.

[29] Guillaume J Filion, Joke G van Bemmel, Ulrich Braunschweig, Wendy Talhout, Jop Kind, Lucas D Ward, Wim Brugman, Inês J de Castro, Ron M Kerkhoven, Harmen J Bussemaker, et al. Systematic protein location mapping reveals five principal chromatin types in drosophila cells. *Cell*, 143(2):212–224, 2010.

[30] Irina Solovei, Katharina Thanisch, and Yana Feodorova. How to rule the nucleus: divide et impera. *Current opinion in cell biology*, 40:47–59, 2016.

[31] Steven W Criscione, Marco De Cecco, Benjamin Siranosian, Yue Zhang, Jill A Kreiling, John M Sedivy, and Nicola Neretti. Reorganization of chromosome architecture in replicative cellular senescence. *Science advances*, 2(2):e1500882, 2016.

[32] Elphège P Nora, Bryan R Lajoie, Edda G Schulz, Luca Giorgetti, Ikuhiro Okamoto, Nicolas Servant, Tristan Piolot, Nynke L Van Berkum, Johannes Meisig, John Sedat, et al. Spatial partitioning of the regulatory landscape of the x-inactivation centre. *Nature*, 485(7398):381–385, 2012.

[33] Borbala Mifsud, Filipe Tavares-Cadete, Alice N Young, Robert Sugar, Stefan Schoenfelder, Lauren Ferreira, Steven W Wingett, Simon Andrews, William Grey, Philip A Ewels, et al. Mapping long-range promoter contacts in human cells with high-resolution capture hi-c. *Nature genetics*, 47(6):598–606, 2015.

[34] Zhonghui Tang, Oscar Junhong Luo, Xingwang Li, Meizhen Zheng, Jacqueline Jufen Zhu, Przemyslaw Szalaj, Pawel Trzaskoma, Adriana Magalska, Jakub Wlodarczyk, Blazej Ruszczycki, et al. Ctcf-mediated human 3d genome architecture reveals chromatin topology for transcription. *Cell*, 163(7):1611–1627, 2015.

[35] Christian Lanctôt, Thierry Cheutin, Marion Cremer, Giacomo Cavalli, and Thomas Cremer. Dynamic genome architecture in the nuclear space: regulation of gene expression in three dimensions. *Nature Reviews Genetics*, 8(2):104–115, 2007.

[36] Jesse R Dixon, Siddarth Selvaraj, Feng Yue, Audrey Kim, Yan Li, Yin Shen, Ming Hu, Jun S Liu, and Bing Ren. Topological domains in mammalian genomes identified by analysis of chromatin interactions. *Nature*, 485(7398):376–

380, 2012.

[37] Johan H Gibcus, Kumiko Samejima, Anton Goloborodko, Itaru Samejima, Natalia Naumova, Johannes Nuebler, Masato T Kanemaki, Linfeng Xie, James R Paulson, William C Earnshaw, et al. A pathway for mitotic chromosome formation. *Science*, 359(6376):eaao6135, 2018.

[38] Nike Walther, M Julius Hossain, Antonio Z Politi, Birgit Koch, Moritz Kueblbeck, Øyvind Ødegård-Fougner, Marko Lampe, and Jan Ellenberg. A quantitative map of human condensins provides new insights into mitotic chromosome architecture. *Journal of Cell Biology*, 217(7):2309–2328, 2018.

[39] Joel C Eissenberg, Tharappel C James, Dawn M Foster-Hartnett, Thomas Hartnett, Vivian Ngan, and SC Elgin. Mutation in a heterochromatin-specific chromosomal protein is associated with suppression of position-effect variegation in drosophila melanogaster. *Proceedings of the National Academy of Sciences*, 87(24):9923–9927, 1990.

[40] Andrew J Bannister, Philip Zegerman, Janet F Partridge, Eric A Miska, Jean O Thomas, Robin C Allshire, and Tony Kouzarides. Selective recognition of methylated lysine 9 on histone h3 by the hp1 chromo domain. *Nature*, 410(6824):120–124, 2001.

[41] Daniele Canzio, Adam Larson, and Geeta J Narlikar. Mechanisms of functional promiscuity by hp1 proteins. *Trends in cell biology*, 24(6):377–386, 2014.

[42] Sinan Kilic, Andreas L Bachmann, Louise C Bryan, and Beat Fierz. Multivalency governs hp1α association dynamics with the silent chromatin state. *Nature communications*, 6(1):1–11, 2015.

[43] Shelagh Boyle, Ilya M Flyamer, Iain Williamson, Dipta Sengupta, Wendy A Bickmore, and Robert S Illingworth. A central role for canonical prc1 in shaping the 3d nuclear landscape. *Genes & development*, 34(13-14):931–949, 2020.

[44] Emanuela Bianchi, Piero Tartaglia, Emanuela Zaccarelli, and Francesco Sciortino. Theoretical and numerical study of the phase diagram of patchy colloids: Ordered and disordered patch arrangements. *The Journal of chemical physics*, 128(14):144504, 2008.

[45] PIC Teixeira and JM Tavares. Phase behaviour of pure and mixed patchy colloids—theory and simulation. *Current Opinion in Colloid & Interface Science*, 30:16–24, 2017.

[46] Zhenli Zhang and Sharon C Glotzer. Self-assembly of patchy particles. *Nano letters*, 4(8):1407–1413, 2004.

[47] Diana Fusco and Patrick Charbonneau. Crystallization of asymmetric patchy models for globular proteins in solution. *Physical Review E*, 88(1):012721, 2013.

[48] CA Brackley. Polymer compaction and bridging-induced clustering of protein-inspired patchy particles. *Journal of Physics: Condensed Matter*, 32(31):314002, 2020.

[49] Robert S Illingworth. Chromatin folding and nuclear architecture: Prc1 function in 3d. *Current Opinion in Genetics & Development*, 55:82–90, 2019.

[50] Shan-Fu Wu, Haiying Zhang, and Bradley R Cairns. Genes for embryo development are packaged in blocks of multivalent chromatin in zebrafish sperm. *Genome research*, 21(4):578–589, 2011.

[51] Oliver Wiese, Davide Marenduzzo, and Chris A Brackley. Nucleosome positions alone can be used to predict domains in yeast chromosomes. *Proceedings of the National Academy of Sciences*, 116(35):17307–17315, 2019.

[52] Surya K Ghosh and Daniel Jost. How epigenome drives chromatin folding and dynamics, insights from efficient coarse-grained models of chromosomes. *PLoS computational biology*, 14(5):e1006159, 2018.

[53] Andrea M Chiariello, Carlo Annunziatella, Simona Bianco, Andrea Esposito, and Mario Nicodemi. Polymer physics of chromosome large-scale 3d organisation. *Scientific reports*, 6(1):29775, 2016.

[54] Julio Mateos-Langerak, Manfred Bohn, Wim de Leeuw, Osdilly Giromus, Erik MM Manders, Pernette J Verschure, Mireille HG Indemans, Hinco J Gierman, Dieter W Heermann, Roel Van Driel, et al. Spatially confined folding of chromatin in the interphase nucleus. *Proceedings of the National Academy of Sciences*, 106(10):3812–3817, 2009.

[55] John F Marko and Eric D Siggia. Polymer models of meiotic and mitotic chromosomes. *Molecular biology of the cell*, 8(11):2217–2231, 1997.

[56] Mariano Barbieri, Mita Chotalia, James Fraser, Liron-Mark Lavitas, Josée Dostie, Ana Pombo, and Mario Nicodemi. Complexity of chromatin folding is captured by the strings and binders switch model. *Proceedings of the National Academy of Sciences*, 109(40):16173–16178, 2012.

[57] Chris A Brackley, Stephen Taylor, Argyris Papantonis, Peter R Cook, and Davide Marenduzzo. Nonspecific bridging-induced attraction drives clustering of dna-binding proteins and genome organization. *Proceedings of the National Academy of Sciences*, 110(38):E3605–E3611, 2013.

[58] J Johnson, CA Brackley, PR Cook, and D Marenduzzo. A simple model for dna bridging proteins and bacterial or human genomes: bridging-induced attraction and genome compaction. *Journal of Physics: Condensed Matter*, 27(6):064119, 2015.

[59] Chris A Brackley, Benno Liebchen, Davide Michieletto, Francois Mouvet, Peter R Cook, and Davide Marenduzzo. Ephemeral protein binding to dna shapes stable nuclear bodies and chromatin domains. *Biophysical Journal*, 112(6):1085–1093, 2017.

[60] Marco Ancona and Chris A Brackley. Simulating the chromatin-mediated phase separation of model proteins with multiple domains. *Biophysical Journal*, 121(13):2600–2612, 2022.

[61] Daniel Jost, Pascal Carrivain, Giacomo Cavalli, and Cédric Vaillant. Modeling epigenome folding: formation and dynamics of topologically associated chromatin domains. *Nucleic acids research*, 42(15):9553–9561, 2014.

[62] Martin Falk, Yana Feodorova, Natalia Naumova, Maxim Imakaev, Bryan R Lajoie, Heinrich Leonhardt, Boris Joffe, Job Dekker, Geoffrey Fudenberg, Irina Solovei, et al. Heterochromatin drives compartmentalization of inverted and conventional nuclei. *Nature*, 570(7761):395–399, 2019.

[63] Simona Bianco, Darío G Lupiáñez, Andrea M Chiariello, Carlo Annunziatella, Katerina Kraft, Robert Schöpflin, Lars Wittler, Guillaume Andrey, Martin Vingron, Ana Pombo, et al. Polymer physics predicts the effects of structural variants on chromatin architecture. *Nature genetics*, 50(5):662–667, 2018.

[64] Ajoy Maji, Jahir A Ahmed, Subhankar Roy, Buddhapriya Chakrabarti, and Mithun K Mitra. A lamin-associated chromatin model for chromosome organization. *Biophysical Journal*, 118(12):3041–3050, 2020.

[65] Anton Goloborodko, John F Marko, and Leonid A Mirny. Chromosome compaction by active loop extrusion. *Biophysical journal*, 110(10):2162–2168, 2016.

[66] Geoffrey Fudenberg, Maxim Imakaev, Carolyn Lu, Anton Goloborodko, Nezar Abdennur, and Leonid A Mirny. Formation of chromosomal domains by loop extrusion. *Cell reports*, 15(9):2038–2049, 2016.

[67] Mattia Conte, Luca Fiorillo, Simona Bianco, Andrea M Chiariello, Andrea Esposito, and Mario Nicodemi. Polymer physics indicates chromatin folding variability across single-cells results from state degeneracy in phase separation. *Nature communications*, 11(1):3289, 2020.

[68] Mattia Conte, Ehsan Irani, Andrea M Chiariello, Alex Abraham, Simona Bianco, Andrea Esposito, and Mario Nicodemi. Loop-extrusion and polymer phase-separation can co-exist at the single-molecule level to shape chromatin folding. *Nature Communications*, 13(1):4070, 2022.

[69] Sangram Kadam, Kiran Kumari, Vinoth Manivannan, Shuvadip Dutta, Mithun K Mitra, and Ranjith Padinhateeri. Predicting scale-dependent chromatin polymer properties from systematic coarse-graining. *Nature Communications*, 14(1):4108, 2023.

[70] Stephanie Portillo-Ledesma, Suckwoo Chung, Jill Hoffman, and Tamar Schlick. Regulation of chromatin architecture by transcription factor binding. *Elife*, 12:RP91320, 2024.

[71] Sarah G Swygert, Dejun Lin, Stephanie Portillo-Ledesma, Po-Yen Lin, Dakota R Hunt, Cheng-Fu Kao, Tamar Schlick, William S Noble, and Toshio Tsukiyama. Local chromatin fiber folding represses transcription and loop extrusion in quiescent cells. *Elife*, 10:e72062, 2021.

[72] Mario Nicodemi, Barbara Panning, and Antonella Prisco. A thermodynamic switch for chromosome colocalization. *Genetics*, 179(1):717–721, 2008.

[73] Mario Nicodemi and Antonella Prisco. Thermodynamic pathways to genome spatial organization in the cell nucleus. *Biophysical journal*, 96(6):2168–2177, 2009.

[74] Thomas Cremer and Christoph Cremer. Chromosome territories, nuclear architecture and gene regulation in mammalian cells. *Nature reviews genetics*, 2(4):292–301, 2001.

[75] Chris A Brackley, James Johnson, Steven Kelly, Peter R Cook, and Davide Marenduzzo. Simulated binding of transcription factors to active and inactive regions folds human chromosomes into loops, rosettes and topological domains. *Nucleic acids research*, 44(8):3503–3512, 2016.

[76] Davide Michieletto, Enzo Orlandini, and Davide Marenduzzo. Polymer model with epigenetic recoloring reveals a pathway for the de novo establishment and 3d organization of chromatin domains. *Physical Review X*, 6(4):041047, 2016.

[77] Davide Michieletto, Michael Chiang, Davide Coli, Argyris Papantonis, Enzo Orlandini, Peter R Cook, and Davide Marenduzzo. Shaping epigenetic memory via genomic bookmarking. *Nucleic acids research*, 46(1):83–93, 2018.

[78] Michele Di Pierro, Bin Zhang, Erez Lieberman Aiden, Peter G Wolynes, and José N Onuchic. Transferable model for chromosome architecture. *Proceedings of the National Academy of Sciences*, 113(43):12168–12173, 2016.

[79] Michele Di Pierro, Ryan R Cheng, Erez Lieberman Aiden, Peter G Wolynes, and José N Onuchic. De novo prediction of human chromosome structures: Epigenetic marking patterns encode genome architecture. *Proceedings of the National Academy of Sciences*, 114(46):12126–12131, 2017.

[80] Yifeng Qi and Bin Zhang. Predicting three-dimensional genome organization with chromatin states. *PLoS computational biology*, 15(6):e1007024, 2019.

[81] Yifeng Qi, Alejandro Reyes, Sarah E Johnstone, Martin J Aryee, Bradley E Bernstein, and Bin Zhang. Data-driven polymer model for mechanistic exploration of diploid genome organization. *Biophysical Journal*, 119(9):1905–1916, 2020.

[82] Sougata Guha and Mithun K Mitra. Multivalent binding proteins can drive collapse and reswelling of chromatin in confinement. *Soft Matter*, 19(1):153–163, 2023.

[83] Isha Malhotra, Bernardo Oyarzún, and Bortolo Matteo Mognetti. Unfolding of the chromatin fiber driven by overexpression of noninteracting bridging factors. *Biophysical Journal*, 120(7):1247–1256, 2021.

[84] Ran Yan, Chaonan Zhao, and Nanrong Zhao. Attractive crowding effect on passive and active polymer looping kinetics. *The Journal of Chemical Physics*, 160(13):134902, 2024.

[85] Kurt Kremer and Gary S Grest. Dynamics of entangled linear polymer melts: A molecular-dynamics simulation. *The Journal of Chemical Physics*, 92(8):5057–5086, 1990.

[86] John D Weeks, David Chandler, and Hans C Andersen. Role of repulsive forces in determining the equilibrium structure of simple liquids. *The Journal of chemical physics*, 54(12):5237–5247, 1971.

[87] Keith Roberts, Bruce Alberts, Alexander Johnson, Peter Walter, and Tim Hunt. Molecular biology of the cell. *New York: Garland Science*, 32(2), 2002.

[88] Claudia Cattoglio, Iryna Pustova, Nike Walther, Jaclyn J Ho, Merle Hantsche-Grininger, Carla J Inouye, M Julius Hossain, Gina M Dailey, Jan Ellenberg, Xavier Darzacq, et al. Determining cellular ctcf and cohesin abundances to constrain 3d genome models. *Elife*, 8:e40164, 2019.

[89] Shinichi Machida, Yoshimasa Takizawa, Masakazu Ishimaru, Yukihiko Sugita, Satoshi Sekine, Jun-ichi Nakayama, Matthias Wolf, and Hitoshi Kurumizaka. Structural basis of heterochromatin formation by human hp1. *Molecular cell*, 69(3):385–397, 2018.

[90] Won-Ki Cho, Jan-Hendrik Spille, Micca Hecht, Choongman Lee, Charles Li, Valentin Grube, and Ibrahim I Cisse. Mediator and rna polymerase ii clusters associate in transcription-dependent condensates. *Science*, 361(6400):412–415, 2018.

[91] Patrick Cramer. Organization and regulation of gene transcription. *Nature*, 573(7772):45–54, 2019.

[92] Denes Hnisz, Krishna Shrinivas, Richard A Young, Arup K Chakraborty, and Phillip A Sharp. A phase separation model for transcriptional control. *Cell*, 169(1):13–23, 2017.